Journal of Oceanology and Limnology
Vol. 44, No. 3, pp. 1224-1238, 2026
https://doi.org/10.1007/s00343-025-5123-z

Research Paper

Morphology and phylogeny of the rediscovered *Prorocentrum formosum* from the Zhongsha Islands, South China Sea*

Jingyi CEN[1], Hang XIE[1], Yuan HUANG[1], Linjian OU[1], Songhui LÜ[1, **], Jianyan WANG[2, **]

[1] *Key Laboratory of Eutrophication and Red Tide Prevention of Guangdong Higher Education Institutes, College of Life Science and Technology, and Southern Marine Science and Engineering Guangdong Laboratory (Zhuhai), Jinan University, Guangzhou 510632, China*

[2] *Department of Life Sciences, Natural History Museum of China, Beijing 100050, China*

Received Apr. 18, 2025; accepted in principle Jun. 23, 2025; accepted for publication Aug. 5, 2025

Abstract A strain of benthic dinoflagellate *Prorocentrum formosum* was isolated from the Anding Lianjiao (Contiguous Reef) (also known as Addington Shoal), Zhongsha Islands. Morphological observation using light and scanning electron microscopy revealed vegetative cells measuring 24–27 μm in length and 17–22 μm in width, which displayed an asymmetrical oval shape with smooth surfaces. The left and right valves contained two distinct types of radially arranged pores with differing diameters, characterized by sparsely distributed marginal pores and a seamless connection to the parallel horizontal intercalary band. The periflagellar area comprised 9 platelets arranged in a wide V-shape, containing both larger flagellar pores and smaller accessory pores. Phylogenetic analysis based on ITS and LSU rRNA gene sequences confirmed its classification within *Prorocentrum*, with strong bootstrap support (94% for ITS; 98% for LSU) and posterior probabilities (0.97 for ITS; 1.0 for LSU). Genetic distance analysis showed its closest relationship to *Prorocentrum elegans* (P=0.359 for ITS; P=0.118 for LSU). HPLC analysis detected chlorophyll *a*, chlorophyll c_2, peridinin, diadinoxanthin, and diatoxanthin. Although trace levels of okadaic acid (OA) were detected in the initial cultures, its production was no longer observed after prolonged cultivation of the strain. Toxicity tests demonstrated 72- and 96-h mortality rates of 18.75%±1.07% and 34.54%±2.71% in *Brachionus plicatilis* at 2 660 cells/mL, whereas *Artemia salina* exhibited no mortality after 96-h exposure. Hemolytic activity was not detected in algal extracts. This study provides the first molecular sequences of *P. formosum*.

Keyword: *Prorocentrum formosum*; okadaic acid; morphology; phylogeny; Zhongsha Islands

1 INTRODUCTION

The genus *Prorocentrum* was established by Ehrenberg in 1834, with *Prorocentrum micans* as the type species (Fukuyo, 1981; Tillmann et al., 2019). Currently, a total of 138 species have been described within the genus, of which 85 are taxonomically accepted species according to AlgaeBase (Guiry and Guiry, 2025). Most *Prorocentrum* species are typically planktonic in nature, whereas approximately 35 are benthic or epibenthic (Hoppenrath et al., 2013; Zhang et al., 2015; Nascimento et al., 2017; Verma et al., 2019; Nishimura et al., 2020; Zou et al., 2022). These benthic species inhabit diverse substrates, including macroalgae, seagrass, corals, marine sediments, and floating detrital aggregates (Faust, 1990, 1993a, b; Grzebyk et al., 1998). *Prorocentrum* species are distributed globally, primarily in tropical and subtropical coastal regions (Faust, 1991; Murray et al., 2007; Faust et al., 2008; Chomérat et al., 2010, 2011).

* Supported by the National Key Research and Development (R&D) Program of China (No. 2022YFC3105200), the Guangdong Provincial Key R&D Program (No. 2023B1111050011), the National Natural Science Foundation of China (Nos. 41906112, 41976133, 42276157), and the Beijing Natural Science Foundation (No. 8232026)

** Corresponding authors: lusonghui1963@163.com; wjy198530@163.com

The morphology of *Prorocentrum* is defined by two large valves, the absence of a sulcus, and an apical flagellar insertion (Dodge, 1975). A taxonomically critical feature is the periflagellar region, a complex structure containing two pores at the anterior end of the right valve, surrounded by 5–14 smaller platelets (Hoppenrath et al., 2013). Key morphological traits used for identifying *Prorocentrum* species include cell size, cell symmetry, thecal plate ornamentation (e.g., presence or absence of apical spines, plate depressions, shape and distribution of pores), and periflagellar region morphology (Tomas, 1996; Hoppenrath et al., 2013). Despite its apparently simple cellular organization, *Prorocentrum* taxonomy faces challenges due to intraspecific morphological variation and the occurrence of cryptic species (Leander and Hoppenrath, 2008; Han et al., 2016; Nascimento et al., 2017; Chomérat et al., 2019; Lim et al., 2019).

The detailed structural features of the periflagellar region serve as critical diagnostic characters for species identification. While morphological descriptions are increasingly supported by ultrastructural observations of the periflagellar region, many original species descriptions, particularly those lacking cultured strains, have not accurately characterized this region (Hoppenrath et al., 2013; Gómez and Gast, 2022).

Thirteen *Prorocentrum* species are recognized as harmful algal bloom formers and included in the IOC-UNESCO Taxonomic Reference List of Harmful Microalgae (Lundholm et al., 2025). These species produce diverse toxins, including OA, its analogues, and other bioactive compounds such as dinophysistoxins (DTX-1, DTX-2), borbotoxins, fast-acting toxins, and hemolytic toxins, which induce diarrhetic shellfish poisoning (DSP) to humans via trophic transfer (Hoppenrath et al., 2013). OA, along with DTXs like DTX-1 and DTX-2, are primary inducers of DSP (Alexander et al., 2019). Their lipophilic properties facilitate bioaccumulation in marine organism lipid tissues, impeding metabolic detoxification (Bauder et al., 2001). OA and DTXs function by inhibiting the effects of serine/threonine protein phosphatases 1 and 2A (PP1 and PP2A) (Takai et al., 1992), which in turn disrupts various cellular functions (Bialojan et al., 1988; Vale and Botana, 2008; Louzao et al., 2015). To date, at least eight *Prorocentrum* species (*P. faustiae*, *P. caipirignum*, *P. lima*, *P. concavum*, *P. steidingerae*, *P.* cf. *fukuyoi*, *P. hoffmannianum*, *P. leve*) in the genus *Prorocentrum* have been verified to produce OA (Hoppenrath et al., 2013; Zou et al., 2022; www.marinespecies.org/). Simultaneously, OA, DTX-1, and a DTX analogue were identified in *P. lima* from the Xisha (or known as Paracel) Islands (Zou et al., 2022). Recently, the first benthic dinoflagellate bloom caused by *P. concavum* in Hainan Island was reported (Zou et al., 2020), highlighting the imperative to study the potentially toxin-producing capabilities of these *Prorocentrum* strains.

Prorocentrum formosum M. A. Faust, 1993 was first identified from the Lair and Lair Channel, Twin Cays, Belize. This photosynthetic species has small, oval cells measuring 25–28 μm in length and 15–16 μm in width. The valves are smooth, with 42–55; the apical area of the left valve is either flat or inclined. The right valve features a V-shaped periflagellar region composed of 5–6 platelets. It lacks an apical pore but has a large flagellar pore and a prominent apical plate. The intercalary band is transversely striated (Faust, 1993a). Since its original description, *P. formosum* has been recorded in Malaysian waters, though no molecular data have been reported for this species (Faust, 1993a; Mohammad-Noor et al., 2007).

A *P. formosum* strain isolated from the Zhongsha Islands, South China Sea, was identified through integrated morphological and molecular analyses (ITS/LSU rRNA gene sequencing). LC-MS analysis confirmed OA production, while toxicity assessments evaluated hemolytic activity and acute toxicity using standardized bioassays.

2 MATERIAL AND METHOD

2.1 Sampling location and establishing cultures

Benthic dinoflagellates were collected from macroalgal substrates on 22 May 2019 at Anding Lianjiao (Contiguous Reef) (also known as Addington Shoal), Zhongsha Islands, China (114°27.727′E, 15°36.155′N) at a depth of 19 m via diving (Fig.1). Single cell of *Prorocentrum* was isolated under an Olympus BX61 (Olympus, Japan) light microscope using micropipette aspiration. Isolates were aseptically transferred to 96-well culture plates containing L1 medium (salinity 30). The monoclonal *P. formosum* strain was maintained in the Algal Culture Collection of Jinan University's Red Tide and Marine Biology Research Center, cultured under 12-h:12-h LD cycle with 100-μmol photons/(m^2·s) illumination at 25 °C.

2.2 Morphological and structural observation using light and scanning electron microscopy

Cells of *P. formosum* were examined under a

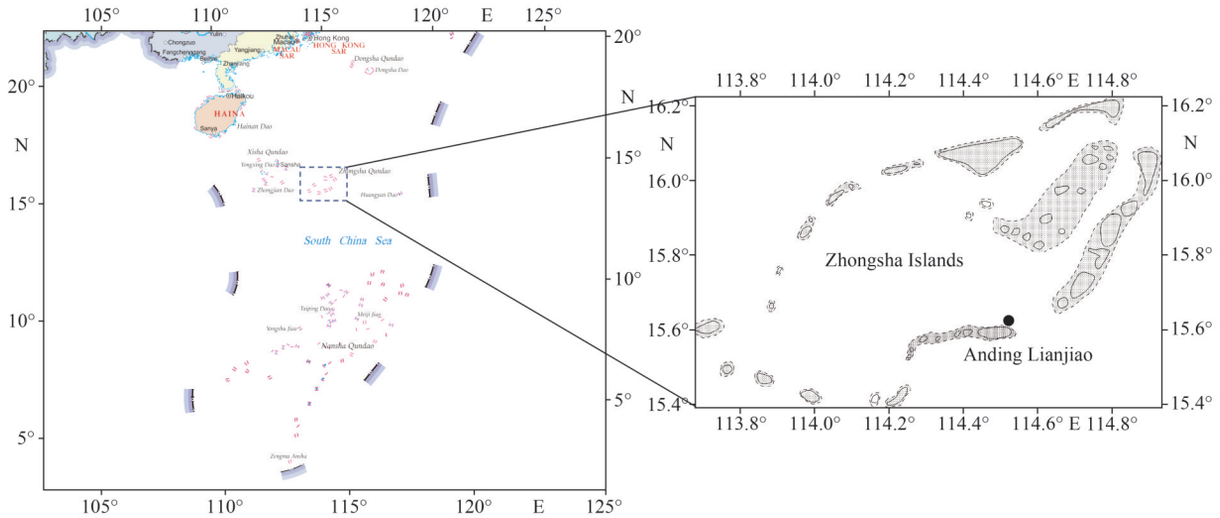

Fig.1 Map of Zhongsha Islands showing the locations where *P. formosum* was isolated from

The black spot is the sampling location.

light microscope (BX61, Olympus, Japan) equipped with a digital camera (QImaging Retiga 4000R, British Columbia, Canada). Live cell images were captured at 400× magnification using Image-Pro Plus 6.0 software, with cell length and width measured from 30 randomly selected individuals. To investigate the morphology and distribution of chloroplasts and the nucleus, cells were stained with Fluorescent Brightener 28 (Sigma, USA) and SYBR Safe DNA gel stain (Invitrogen, Thermo Fisher Scientific, USA) and then imaged at 1 000× magnification.

Scanning Electron Microscopy (SEM) was employed for a more detailed morphological exploration of algal cells. The sample preparation for SEM was followed the protocol described in Lim et al. (2019). Cells in the exponential growth phase were fixed in glutaraldehyde in a final concentration of 2.5% at 4 °C overnight. The fixed sample was dehydrated using a series of ethanol gradients (10%, 30%, 50%, 70%, and 90%), and this step was repeated three times with 100% ethanol for 15 min each. After dehydration, samples were dried in a CO_2 critical point dryer (CPD 300, Leica, Wetzlar, Germany), and then coated with a gold layer using the Leica EM SCD 500 (Leica, Wetzlar, Germany). Final observations were conducted using a Zeiss Ultra 55 field-emission SEM (Carl Zeiss, Germany).

2.3 Molecular characterization: DNA extraction, PCR amplification and sequencing, phylogenetic analysis

One milliliter of *P. formosum* algal culture in exponential growth phase was collected by centrifugation (12 000×*g*, 4 °C, 2 min) for DNA extraction. The genomic DNA was extracted using the MiniBEST Universal DNA Extraction Kit (TaKaRa, Tokyo, Japan) following the manufacturer's instructions. The partial ITS rDNA and LSU rDNA were amplified by the primers ITS1F/ITS2R to target the ITS domain, and primers D1R/D3B for the D1/D3 region of the 28S rRNA gene (Scholin et al., 1994; Pin et al., 2001). The PCR mixture comprised of 2-μL DNA extract, 22-μL sterile Milli-Q water, 1 μL of each primer at 1-μmol/L concentration, and 25 μL of the 2X Accurate Taq Master Mix (Accurate Biotechnology Co., Ltd.), totaling 50 μL. The PCR protocol was as follows: denaturation was started at 94 °C for 4 min, followed by 36 cycles where denaturation was performed at 94 °C for 20 s, annealing was conducted at 56 °C for 30 s, and extension was carried out at 72 °C for 1.5 min. The process was concluded with a final extension at 72 °C for 10 min (Zou et al., 2020). The PCR product was sequenced at Sangon Bioengineering Co., Ltd.

For phylogenetic analysis, GenBank sequences of *Prorocentrum* species showing >97% similarity to *P. formosum* were retrieved. The target sequences were then subjected to multiple alignments using the online tool, MUSCLE (Edgar, 2004). Pairwise genetic distances were computed with MUSCLE and MEGA-X (Kimura 2 parameter model) (Kumar et al., 2018). For the phylogenies of *P. formosum*, construct Maximum Likelihood (ML) trees were constructed using RAxML-HPC2 on XSEDE v. 8.2.12 with

1 000 bootstrap replicates (Stamatakis, 2014). The most suitable model is chosen based on the Akaike Information Criterion using MrModeltest 2.3. With this model, a Bayesian Inference (BI) tree was generated via MrBayes 3.2.7, running for 10 000 000 iterations at 100-generation intervals (Ronquist and Huelsenbeck, 2003). Trees and associated confidence values are visualized using MEGA X and Tree View software (Page, 1996).

2.4 Toxins extraction and analysis

Prorocenturum formosum was cultured in a 2-L Erlenmeyer flasks for toxin extraction. Cells in the late exponential growth phase were harvested by centrifuging at 12 000×*g* for 10 min and then transferred to 50-mL centrifuge tubes maintained at 4 ℃. The cell precipitate was dissolved in 3 mL of 95% methanol, and the mixture was ultra-sonicated for 40 min in an ice bath. Supernatant was then collected by centrifuging at 12 000×*g* for 10 min at 4 ℃. This step was repeated once more. The supernatant (0.5 mL) was subsequently filtered using a 0.22-μm spin-filters (Pall Corporation, USA), transferred to a 2-mL vial, and stored at -80 ℃ until further HPLC analysis.

Toxin analysis was conducted using an HPLC system (Shimadzu prominence LC-20ADXR) equipped with a 5500 QTRAP LC-MS system (AB Sciex Instruments, Foster City, CA). Toxins were separated using a Phenomenex Kinetex XB-C18 (150 mm× 2.1 mm, 2.6 μm) chromatographic column. The analytical setup for toxin determination included a mobile phase comprising acetonitrile (solvent A) and 0.05% formic acid in water (solvent B). The gradient began with 20% solvent A, ramping up to 90% over 7 min, holding at 90% solvent A for 3 min, and then returning to 20% solvent A within 0.1 min. The sample injection volume was set at 5 μL, with separation taking place at a consistent temperature of 25 ℃ and a flow rate of 0.35 mL/min.

2.5 Pigment composition

The pigment composition of *P. formosum* was analyzed using a Waters E2695 HPLC system (Waters, Milford, USA). The protocol followed Zapata et al. (2000) with modifications: 50-mL algal culture was concentrated and filtered through a 47-mm Whatman GF/F membrane. The membrane was sectioned, transferred to a 15-mL centrifuge tube with 2-mL 95% methanol, and stored at 4 °C for 12 h prior to 30-min sonication. The supernatants were filtered using 0.2-μm spin filters (Pall Corporation, USA), and then transferred to a tube for pigment analysis. A C8 column (150 mm× 4.6 mm, 3.5 μm, by Waters) was used for the chromatographic separation of the pigments. The mobile phase solution A consisted of methanol, acetonitrile, and pyridine water in a 50∶25∶25 (V∶V∶V) ratio, while solution B was a mixture of methanol, acetonitrile, and acetone in a 20∶60∶20 (V∶V∶V) ratio. The injection volume was set at 100 μL with a flow rate of 1 mL/min at 25 ℃. The mobile phase gradient proceeded as follows: (1) 100% solution A, 0% solution B (0 min), (2) 60% solution A, 40% solution B (22 min), (3) solution A 5%, solution B 95% (28 min), (4) solution A 5%, solution B 95% (38 min), and (5) solution A 100%, solution B 0% (40 min). Pigments were identified based on their retention time and spectral characteristics compared to known pigment standards.

2.6 Haemolytic assay and the bioassay toxicity

Hemolytic activity of *P. formosum* was analyzed using exponentially growing cultures (2 264 cells/mL). Cells were centrifuged (5 000×*g*, 10 min) and extracted following Eschbach et al. (2001) with modifications: the pellet was resuspended in 2-mL hemolysis buffer, sonicated at 4 °C for 30 min, and centrifuged. The supernatant was discarded, and the pellet was assayed for hemolytic activity using rabbit erythrocytes (Zhou et al., 2007). The hemolytic toxin in PBS buffer and erythrocytes suspension in PBS buffer were used as blank control, and the erythrocytes mixed with equal volume of 1% Triton X-100 were used as positive control. Cultures of *Prorocentrum obtusidens* (with a concentration of 2 540 cells/mL) were extracted and used as negative control. Each test was conducted in triplicate (Zhou et al., 2007).

Toxicity bioassays of *P. formosum* were performed using *Brachionus plicatilis* and *Artemia salina*, with the culture medium as a blank control. All assays were conducted in triplicate using exponentially growing *P. formosum* cultures. Before testing, both species were starved for 24 h under controlled conditions (25±1 °C, salinity 30). For *B. plicatilis*, 10 per well were exposed in 24-well plates containing 2 mL of test solution supplemented with algal liquid at two densities: 2 660 cells/mL (high-density group) and 555 cells/mL (low-density group). For *A. salina*, 10 per well were exposed in 12-well plates with 5 mL of test solution plus algal suspensions at 5 090 cells/mL (high-group) or 1 200 cells/mL (low-group). Survival was recorded at 3-, 6-, 12-, 24-,

48-, 72-, and 96-h post-exposure (Wang et al., 2023).

The data obtained were analyzed using Origin 2022 for graphical representation and SPSS Statistics 27 for statistical analysis. Differences between groups were determined by one-way ANOVA, and post-hoc comparisons were conducted using Fisher's least significant difference (LSD) test. Significance levels were set at $P<0.05$ and $P<0.01$.

3 RESULT

3.1 Morphological analysis

The cell of *Prorocentrum formosum* is oval and composed of two valves (Fig.2a–b, h). Their valve surfaces are covered with pores (Fig.2h). The cell is slightly asymmetric, with the right apical (or anterior) region being slightly higher than the left in ventral view (Fig.2a–b, d). The cells measure 23.81–27.06 μm in length (mean 25.52±1.01 μm, n=30) and 17.49–21.89 μm in width (mean 19.72±1.35 μm, n=30), with a length-to-width ratio ranging from 1.23 to 1.39 (mean 1.29±0.06, n=30) (Table 1). Under light microscopy, the cells contain numerous irregularly shaped, yellow-brown chloroplasts distributed throughout the cytoplasm (Fig.2a–e), and a posterior nucleus (Fig.2f). No pyrenoid was observed.

Under SEM (Fig.3a–g), the apical region of the cell features a large V-shaped depression on the anterior right valve (Fig.3a). The thecal surface is smooth, lacking pronounced thick flanges on the upper right region or collars on the left valve (Fig.3a–b). Two distinct pore types, varying in diameter, are present on the valve surfaces (Fig.3a–f), primarily distributed along the margins (Fig.3a–d), with no pores in the central area (Fig.3a–b). The periflagellar region is characterized by radial rows of pores (Fig.3a–c). The periflagellar area is located at the apical end of the right valve, characterized by a shallow triangular depression (Fig.3e–g). This region contains both an accessory pore and a flagellar pore, with the accessory pore being significantly smaller than the flagellar pore (Fig.3e). Based on the nomenclature proposed by Hoppenrath et al. (2013), nine periflagellar platelets (1a, 1b, 2, 3, 4, 5, 6, 7, and 8) are identified in this species (Fig.4a, b). The surface of the platelets is predominantly smooth, and platelet 1a exhibits a wing-like structure (Fig.3e & f), adjacent to the accessory pore (Fig.3e–g). The accessory pore is small and often partially obscured by protrusions from platelets 1, 6, and 8 (Fig.3e–g). The flagellar pore is surrounded by protrusions, with an

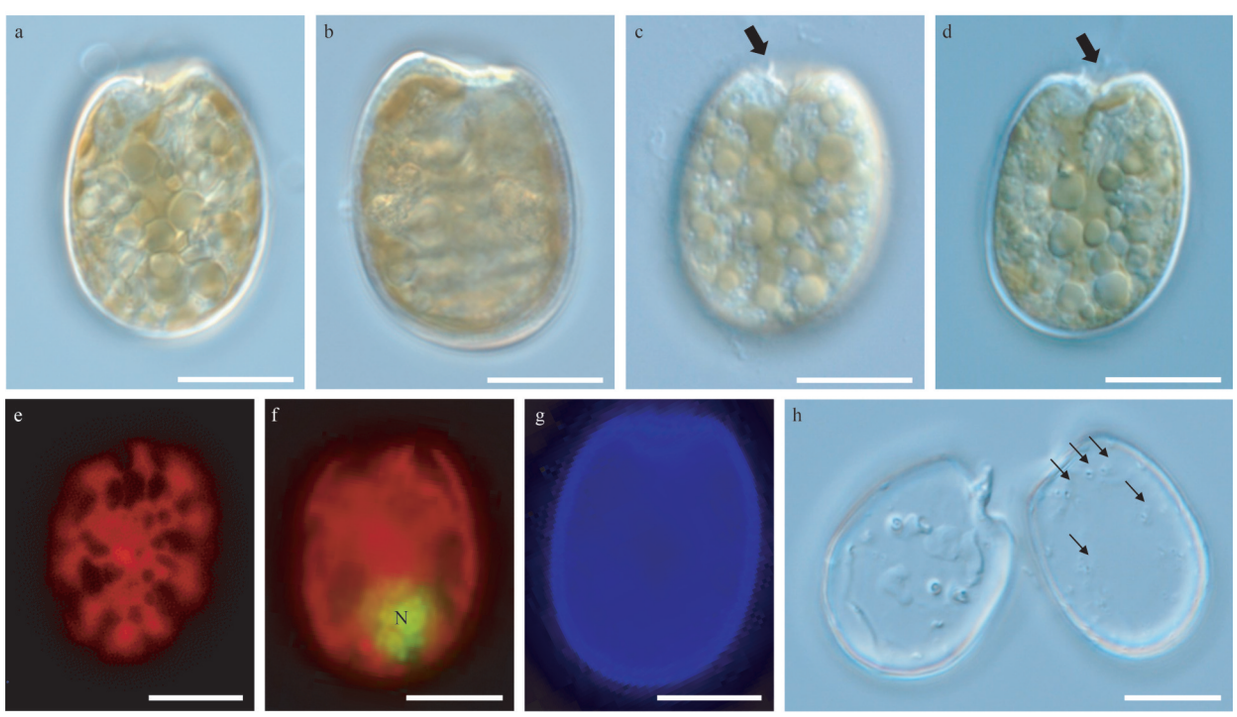

Fig.2 Images of *P. formosum* under light microscope

a–d, h. LM images depicting the left (a) and right (b) valves of the cell; c. prominent lists (arrow); d. wide V-shaped structure (arrow); e–g. fluorescent LM highlighting the chloroplasts (e) and showing the position of the nucleus (f); g. structure of the platelet shell; h. the pores of the shell (arrows). N: nucleus. Scale bars=10 μm.

Table 1 Comparison in morphological features of *P. formosum* with its closely related species

Characteristic	*P. formosum* (ZSG2)	*P. formosum*[a]	*P. formosum*[b]	*P. elegans*[c, d]	*P. emarginatum*[e, f]	*P. fukuyoi*[e, g]	*P. koreanum*[h]
Cell shape	Oval	Oval	Oval to oblong	Oval	Round to oval	Oval to oblong	Drop shaped
Cell symmetry	Asymmetric	Asymmetric	Asymmetric	Asymmetric	Asymmetric	Asymmetric	Asymmetric
Length (μm)	23.81–27.06	25–28	18–21	15–20	30–40	28–42	30.4–44.6
Width (μm)	17.49–21.89	15–16	13–15	10–14	25–35	18–30	21.8–31.5
Periflagellar area	Widely triangular	Nd	Widely triangular	Nd	Deep	Deep	Nd
Periflagellar shape	Wide V-shaped	Wide V-shaped	Wide V-shaped	Wide V-shaped	Narrow V-shaped	Narrow V-shaped	Shallow, V-shaped
Collar on left platelet	No	Nd	No	No	No	No	No
Thick flange	No	No	No	Nd	Yes	Yes	No
Wing-shaped spine	Yes	Nd	Nd	Yes	Yes	Yes	Yes
Protrusions	3	Nd	Nd	No	No	2	No
Number of platelets	9	5–6	5–6	8	9	9	8
Platelet division	1a, 1b	Nd	Nd	Nd	Nd	Nd	Nd
Periflagellar pore	Yes	No	No	Yes	Yes	Yes	Yes
Accessory pore	Yes	No	No	Yes	Yes	Nd	Yes
Theca ornamentation	Smooth	Smooth	Smooth	Smooth	Foveate smooth	Smooth	Nd

Pore pattern	Radial rows	distinct pattern	distinct patter	Apical row	Radial row	No; pore row	Radial row
					Also double row	Scattered	
Marginal pore	No	No	No	Yes	Yes	Nd	No
Platelet center	Devoid	Devoid	Devoid	Devoid	Devoid	Small pores	Large pores
Small pore (μm)	0.06–0.15, *n*=50	<0.01	0.09–0.24	0.12	0.06–0.10	0.1	No
Large pore (μm)	0.20–0.43, *n*=30	0.2	0.29–0.38	0.6	0.18–0.24	0.3	Yes
Intercalary band	Smooth, trans. Straited	Smooth, trans. Straited	Smooth, trans. Straited	Smooth, trans. Straited	Smooth, trans. Straited	Smooth, trans. Straited	Smooth
Pyrenoid	No	No	No	No	Yes	Yes	No
Nucleus shape	Round	Nd	Nd	Teardrop-shaped	Bean-shaped	Round to kidney-shaped	Heart-shaped
Nucleus position	Posterior	Posterior	Posterior	Anterior	Posterior	Posterior	Posterior

[a]: Faust (1993a); [b]: Mohammad-Noor et al. (2007); [c]: Faust (1993b); [d]: David et al. (2014); [e]: Hoppenrath et al. (2013); [f]: Luo et al. (2017); [g]: Murray et al. (2007); [h]: Han et al. (2016). Nd: not determined.

additional protrusion located between platelets 4 and 5 (Fig.3g). The intercalary band displays a smooth surface with broad transverse striations (Fig.3c, d).

3.2 Genetic distance and phylogenetic analysis

LSU and ITS rDNA sequences of strain ZSG2 (Zhongsha Islands, China) were obtained and deposited in GenBank under accession numbers PV524993 and PV524994. These sequences were selected for phylogenetic tree construction. In the LSU rDNA phylogeny (Fig.5), *P. formosum* (strain ZSG2) was resolved as a strong-supported clade (98%/1.0), grouping most closely with *P. rhathymum*, *P. koreanum*, *P. micans*, *P. elegans*, *P. obtusidens*, and *P. cordatum*. Within the ITS phylogenetic tree (Fig.6), *P. formosum* formed a distinct clade with strong bootstrap support (--/1.0), clustering closest to *P. koreanum*, *P. rhathymum*, *P. micans*, *P. elegans*, *P. triestinum*, *P. cordatum*, *P. balticum*, and *P. obtusidens*.

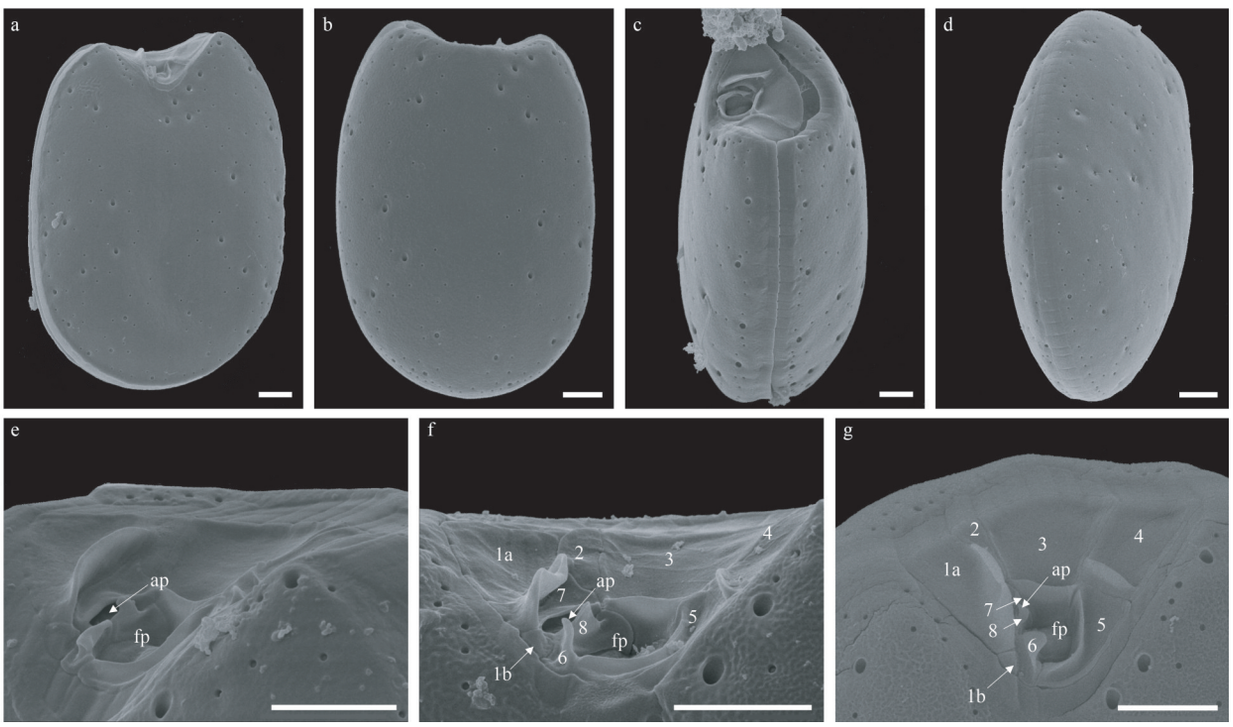

Fig.3 The morphological characters of *P. formosum* based on SEM

a–b. ventral and dorsal views of the right and left valves, respectively, showing the smooth valve surface and two distinct pore sizes distributed along the margins; c–d. lateral view of the cell, highlighting the transversely striated intercalary band; e–g. detailed views of the periflagellar area, showing the flagellar pore (fp), accessory pore (ap), and the arrangement of platelets (numbered according to Hoppenrath et al., (2013)). Scale bars=2 μm.

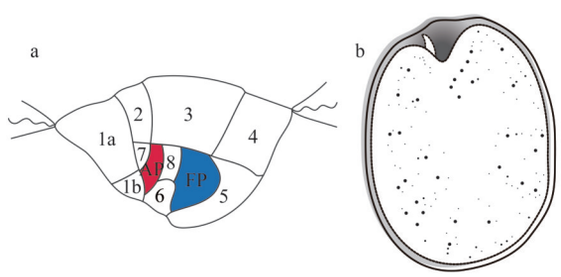

Fig.4 Schematic drawings of *Prorocentrum formosum*

a. periflagellar area, showing the flagellar pore (FP) and accessory pore (AP); b. right plates.

Pairwise genetic distances of the D1–D3 LSU and ITS rDNA sequences were compared among *Prorocentrum* sequences and other related species (Tables 2–3). The interspecies genetic distances within the genus *Prorocentrum*, based on the LSU rDNA sequence, ranged 0.025%–0.158%. The genetic distance of *P. formosum* to its closest relative, *P. elegans*, was 0.134% (11 bp out of 819 bp of LSU rDNA), which is notably higher than the minimum interspecific variability observed within the genus, such as the distance between *P. elegans* KF835600 and *P. elegans* MH381771, which was only 0.002%. In comparison, the genetic distances between *P. formosum* and other *Prorocentrum* species were generally higher, with values ranging from 0.118% to 0.155%. The shortest genetic distance was 0.118%, observed between *P. formosum* and *P. elegans*, which is still higher than the genetic distances fluctuating between 0.053% and 0.080% among recognized distinct species of *Prorocentrum*, such as *P. elegans*, *P. micans*, and *P. koreanum*. These findings indicate a significant genetic divergence between *P. formosum* and the other species within the genus, supporting its classification as a distinct species.

Similar trends were observed for genetic distances based on ITS rDNA sequences, which ranged from 0.016% to 0.449% among *Prorocentrum* species. The closest genetic relationship observed was found between *P. formosum* and *P. elegans* MH356284, with a divergence of 0.364% (31 base pair differences out of 85 bp of ITS rDNA). This genetic divergence is again higher than the minimal interspecific variability within the genus, as seen in distances among other *Prorocentrum* species, which ranged 0.002%–0.304%. The genetic divergence between *P. formosum* and other *Prorocentrum* species, such as *P. cordatum* and *P. obtusidens*, was even more pronounced, with genetic distances reaching up to

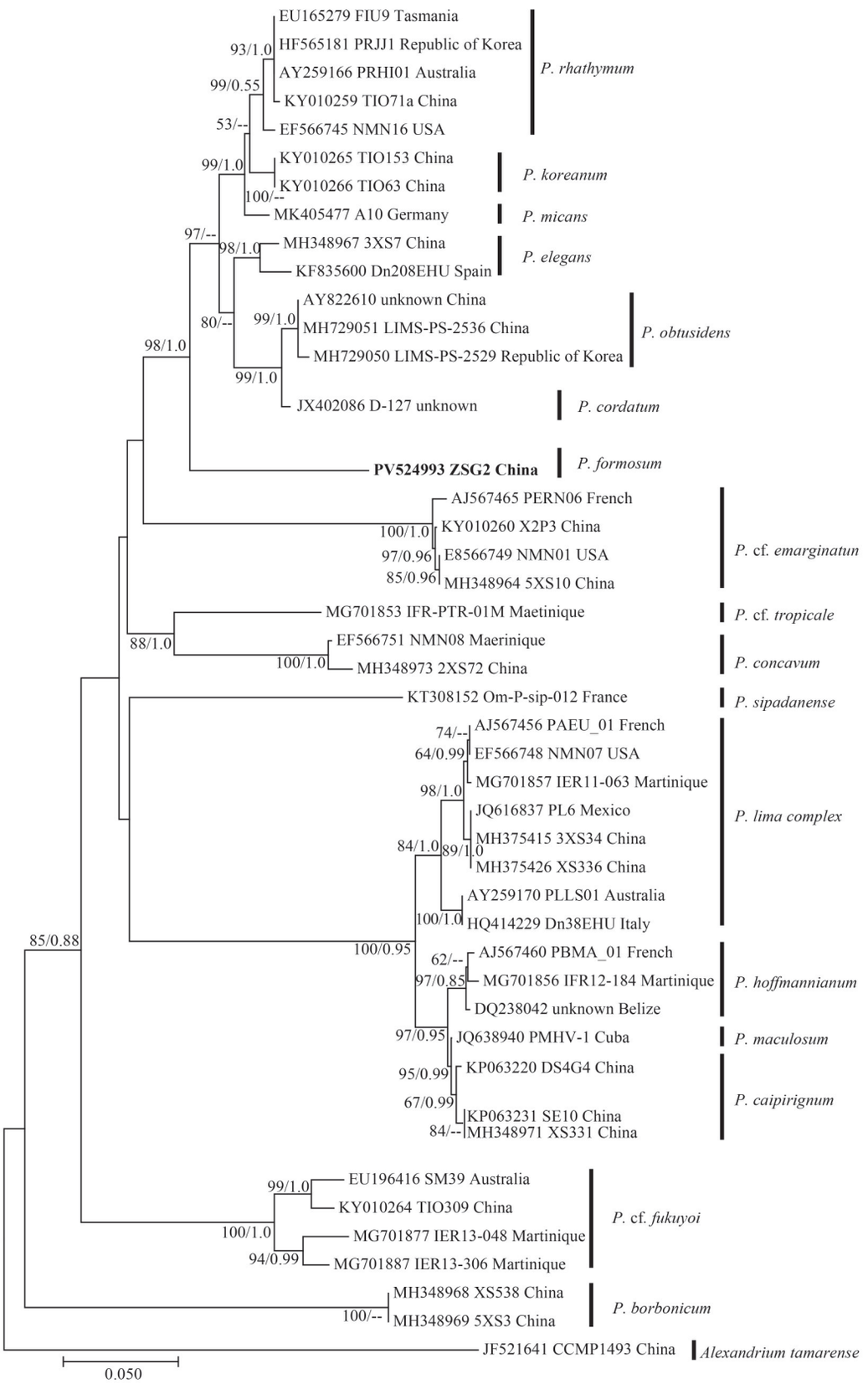

Fig.5 Phylogenetic tree of partial LSU rDNA (D1–D3) sequences of *Prorocentrum* species based on the maximum likelihood (ML) and Bayesian inference (BI)

Alexandrium tamarense (JF521641) is used as the outgroup and sequences obtained in the present study are in bold. Bootstrap values <50% and posterior probabilities <0.5 are not shown.

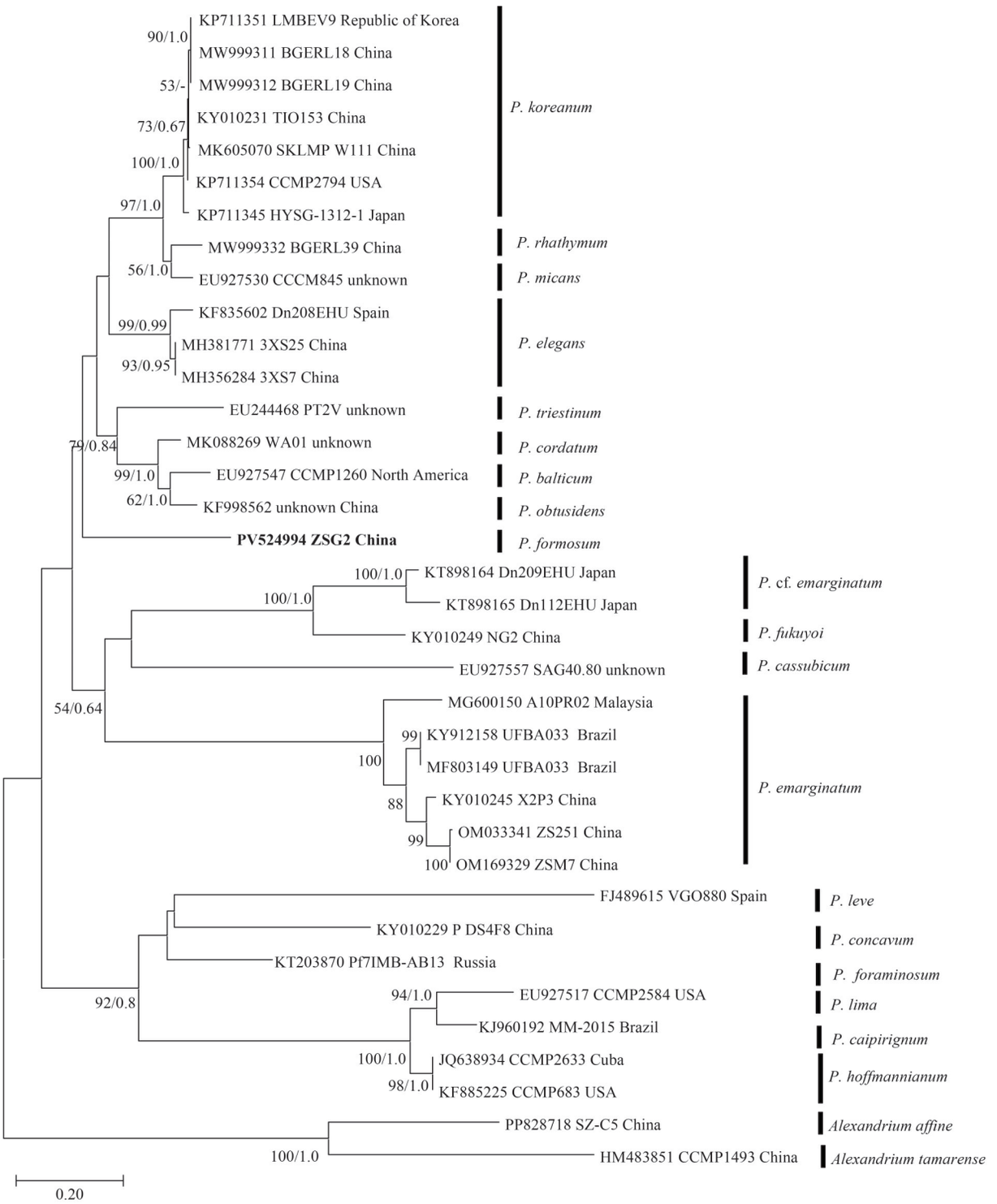

Fig.6 Phylogenetic tree of partial ITS rDNA sequences of *Prorocentrum* species based on the maximum likelihood (ML) and Bayesian inference (BI)

Bootstrap values <50% and posterior probabilities <0.5 are not shown.

0.449% based on ITS sequences. In comparison, genetic distances among other *Prorocentrum* species, such as *P. elegans* and *P. micans*, ranged 0.002%–0.291%, further reinforcing the genetic distinctness of *P. formosum* within the genus *Prorocentrum*.

3.3 Toxin and toxicity analysis

Trace amounts of the lipophilic toxin OA were detected in the initial cell extracts of *P. formosum* during the strain isolation phase via LC-MS.

Table 2 Uncorrected ("p") distance matrix based on D1–D3 LSU rDNA sequences

		1	2	3	4	5	6	7	8	9	10	11	12	13	14	15
1	*P. formosum* ZSG2															
2	*P. elegans* KF835600	0.134														
3	*P.elegans* MH348967	0.118	0.025													
4	*P. cordatum* JX402086	0.138	0.047	0.079												
5	*P. obtusidens* MH729050	0.147	0.065	0.090	0.025											
6	*P. obtusidens* MH729051	0.143	0.060	0.088	0.023	0.002										
7	*P. obtusidens* AY822610	0.145	0.059	0.087	0.023	0.002	0.000									
8	*P. micans* MK405477	0.125	0.053	0.080	0.085	0.102	0.099	0.099								
9	*P. koreanum* KY010266	0.127	0.068	0.078	0.081	0.096	0.094	0.094	0.053							
10	*P. koreanum* KY010265	0.127	0.068	0.078	0.081	0.096	0.094	0.094	0.053	0.000						
11	*P. rhathymum* EF566745	0.121	0.057	0.067	0.081	0.090	0.088	0.087	0.038	0.038	0.038					
12	*P. rhathymum* KY010259	0.124	0.060	0.066	0.080	0.087	0.085	0.084	0.044	0.044	0.044	0.017				
13	*P. rhathymum* AY259166	0.158	0.057	0.088	0.108	0.122	0.119	0.118	0.060	0.062	0.062	0.024	0.003			
14	*P. rhathymum* HF565181	0.123	0.057	0.065	0.078	0.086	0.084	0.083	0.043	0.043	0.043	0.016	0.001	0.002		
15	*P. rhathymum* EU165279	0.155	0.057	0.086	0.110	0.120	0.117	0.116	0.060	0.060	0.060	0.022	0.002	0.002	0.000	

Table 3 Uncorrected ("p") distance matrix based on ITS rDNA sequences

		1	2	3	4	5	6	7	8	9	10	11	12	13	14	15	16	17
1	*P. formosum* ZSG2																	
2	*P. elegans* MH356284	0.364																
3	*P. elegans* MH381771	0.359	0.002															
4	*P. elegans* KF835602	0.399	0.054	0.055														
5	*P. obtusidens* KF998562	0.372	0.304	0.292	0.299													
6	*P. cordatum* MK088269	0.368	0.271	0.260	0.285	0.095												
7	*P. balticum* EU927547	0.372	0.313	0.304	0.317	0.111	0.133											
8	*P. micans* EU927530	0.386	0.251	0.242	0.291	0.260	0.235	0.277										
9	*P. rhathymum* MW999332	0.390	0.240	0.230	0.261	0.267	0.257	0.293	0.099									
10	*P. koreanum* KP711345	0.441	0.260	0.256	0.260	0.268	0.252	0.285	0.106	0.129								
11	*P. koreanum* MK605070	0.431	0.247	0.240	0.257	0.246	0.242	0.273	0.097	0.118	0.018							
12	*P. koreanum* KY010231	0.436	0.244	0.238	0.243	0.247	0.242	0.274	0.101	0.122	0.016	0.002						
13	*P. koreanum* KP711354	0.436	0.252	0.248	0.250	0.260	0.250	0.279	0.106	0.125	0.015	0.004	0.002					
14	*P. koreanum* KP711351	0.449	0.261	0.264	0.259	0.266	0.263	0.292	0.108	0.131	0.019	0.008	0.006	0.008				
15	*P. koreanum* MW999312	0.430	0.252	0.245	0.257	0.245	0.243	0.268	0.101	0.120	0.018	0.007	0.005	0.007	0.000			
16	*P. koreanum* MW999311	0.430	0.252	0.245	0.257	0.245	0.243	0.268	0.101	0.120	0.018	0.007	0.005	0.007	0.000	0.000		
17	*P. triestinum* EU244468	0.435	0.342	0.325	0.347	0.275	0.283	0.296	0.343	0.322	0.322	0.301	0.302	0.310	0.317	0.302	0.302	

However, after prolonged laboratory cultivation, OA and its derivatives DTX-1 and DTX-2 were not detected in the extracts, indicating a loss of toxin production in this strain over time.

The acute toxicity of *P. formosum* on *Brachionus plicatilis* and *Artemia salina* was listed in Table 4. A 96-h exposure test exhibited pronounced detrimental effects of *P. formosum* (harmful algal blooms algae liquid and 10% harmful algal blooms algae liquid) on *Brachionus plicatilis*. At 72 h, the mortality rates were 18.75%±1.07% and 14.79%±1.23% respectively, while at 96 h, the rates increased to 34.54%±2.71%

Table 4 Effects of *P. affine* on the survival of *Brachionus plicatilis* and *Artemia salina* (mortality rate (%))

Time (h)	*Brachionus plicatilis*			*Artemia salina*		
	P. formosum	10% *P. formosum*	Black control	*P. formosum*	10% *P. formosum*	Black control
3	0.00±0.00	0.50±0.70	0.00±0.00	0.00±0.00	0.00±0.00	0.00±0.00
6	1.37±0.98	0.50±0.70	0.00±0.00	0.00±0.00	0.00±0.00	0.00±0.00
12	2.11±1.82	1.14±0.82	3.09±1.03	0.00±0.00	0.00±0.00	0.00±0.00
24	4.91±1.17	3.90±1.81	3.09±1.03	0.00±0.00	0.00±0.00	0.00±0.00
48	11.81±2.61	9.72±1.69	5.56±1.94	6.67±4.71	10.00±0.00	6.67±4.71
72	18.75±1.07	14.79±1.23	8.64±2.55	13.33±4.71	13.33±4.71	6.67±4.71
96	34.54±2.71	25.49±0.45	12.80±3.22	23.33±4.71	13.33±4.71	6.67±4.71

and 25.49%±0.45% respectively, both significantly higher than the blank control group (P<0.05). Regarding *Artemia salina*, no deaths were observed after exposure to *P. formosum* pure cultured algae in 24 h. The mortality rate of *Artemia salina* showed an upward trend in 48 and 96 h without significant differences among the three experimental groups, implying that *P. formosum* did not induce acute lethality in *Artemia salina*. Hemolysis experiments on rabbit blood cells confirmed that *P. formosum* did not pose hemolytic activity (Table 5).

3.4 Pigment analysis

Pigment composition of *P. formosum* (ZSG2) was analyzed through HPLC analysis. Six pigments, chlorophyll c_2 (chl c_2), peridinin, diadinoxanthin, chlorophyll *a* (chl *a*), peridinol, and diatoxanthin, were identified (Fig.7). Among them, chl *a*, peridinin, and diadinoxanthin were the primary pigment constituents. The specific pigment concentrations for the three main pigments were as follows: peridinin (peri) at 0.133±0.010 mg/L, diadinoxanthin (diato) at 0.095±0.008 mg/L, and chl *a* at 0.098± 0.019 mg/L. Some unidentified pigments in trace amounts were also detected.

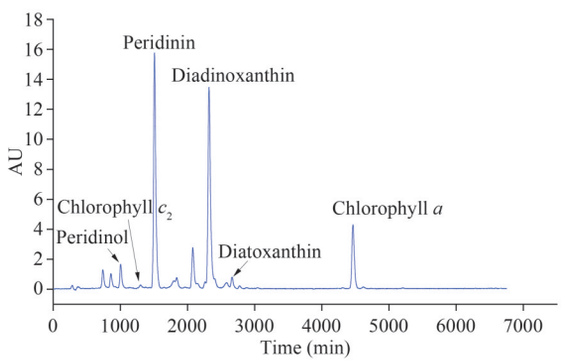

Fig.7 *P. formosum* pigment chromatogram obtained from HPLC analysis

4 DISCUSSION

4.1 Identification of *P. formosum* and its closely related species

Many species of the genus *Prorocentrum* were initially described solely based on morphological characteristics, frequently resulting in taxonomic synonymy among morphologically convergent taxa. For instance, *P. lima* was described by Ehrenberg in 1834 and later revised by Dodge (1975), who documented its morphological plasticity under light microscopy. Subsequent studies demonstrated both high morphological variability and genetic divergence among its morphotypes, suggesting that these morphotypes constitute a *P. lima* species complex despite their genetic distinctness (Zhang et al., 2015). Similarly, *P. mexicanum* and *P. rhathymum* were distinguished primarily by differences in cellular outline and periflagellar area ultrastructure, despite their pronounced morphological overlap (Loeblich et al., 1979; Fukuyo, 1981). This variability led to confusion and multiple descriptions of the same species under different names. The present study integrates morphological observations with molecular phylogenetic evidence, providing conclusive support for the taxonomic validity of *P. formosum* as a distinct species.

Strain ZSG2 was identified as *P. formosum* based on morphological congruence with Faust (1993a)'s original description. Ventral view reveals slight asymmetry with the right apical plate elevated relative to the left (Figs.2a–b, 3a–b), matching

Table 5 The experiment of rabbit blood cell hemolysis

P. formosum	Black control	Negative control	Positive control
6.87%±0.41%	5.60%±0.51%	4.97%±0.09%	94.20%±7.11%

Faust's observation of a flat/inclined left apical margin (figs.14–15 in Faust, 1993a). The valves bear two morphologically distinct pore classes: small pores (0.06–0.15 μm) and large pores (0.20–0.43 μm), showing marginal distribution and a central pore-free zone—consistent with Faust's description of large trichocyst pores and smaller peripheral pores (Faust 1993a). Strain ZSG2 lacks a pyrenoid, a feature confirmed in the original taxon (Faust, 1993a; Mohammad-Noor et al., 2007). The periflagellar area of *P. formosum* is described as V-shaped region of 5–6 platelets lacking an accessory pore, featuring a ventral wing bordering Platelet 1 and a dorsal list on Platelet 4 (Faust, 1993a), along with an annular ridge surrounding the flagellar pore (Faust, 1993a; Mohammad-Noor et al., 2007). Strain ZSG2 recapitulates this platelet configuration, including a ventral flange on Platelet 1 and an angled plate (Figs.3e–g). The accessory pore in Strain ZSG2 did not report by Faust (1993a) and Mohammad-Noor et al. (2007). Due to its inconspicuous positioning, this pore remains indistinct in ventral view (Fig.3g) but becomes discernible at specific angles, appearing as a small aperture obscured by Platelet 1 and protrusions adjacent to the flagellar pore (Fig.3c, e–f). Although *P. formosum* was originally defined by the absence of an accessory pore—a key diagnostic trait distinguishing it from congeners (e.g., *P. elegans*), the periflagellar area morphology of Strain ZSG2 (Fig.3g) and other features align with the species' taxonomic criteria. Consequently, Strain ZSG2 is classified herein as *P. formosum*.

In this study, light microscopy confirmed the absence of a pyrenoid in *P. formosum*, a trait first noted by Faust (1993a) and critical for distinguishing it from *P. mexicanum* and most *Prorocentrum* species, which typically possess this structure (Hoppenrath et al., 2013). Morphologically, *P. formosum* shares a broadly V-shaped periflagellar region with *P. elegans* (Faust, 1993a, b). The *P. formosum* (23.81–27.06 μm in length, 1.23–1.39 length-to-width ratio) displays three protrusions in the periflagellar area (Fig.3) and nine platelets (Fig.3f–g), compared to *P. elegans* (15–20 μm length), which lacks protrusions and possesses eight platelets (Faust, 1993b; Hoppenrath et al., 2013). Additionally, *P. formosum* exhibits a radial pore pattern on its smooth thecal surface (Fig.3a–d), contrasting with the apical row of pores in *P. elegans* (Faust, 1993b). Contrasting with *P. emarginatum* and *P. fukuyoi*, which have narrow V-shaped periflagellar regions with thick flanges and central pyrenoids, *P. formosum* lacks pyrenoids and displays a smooth thecal surface without flanges (Murray et al., 2007; Aligizaki et al., 2009). *P. fukuyoi* displays randomly scattered pores with central platelet aggregation, while *P. formosum* demonstrates radially aligned pore rows and a distinct central pore-free zone (Fig.3a–c) (Murray et al., 2007). The *P. koreanum* differs significantly in cell shape, periflagellar structure, and pore distribution, with large pores concentrated centrally and lacking small pores (Han et al., 2016). Earlier reports suggested *P. formosum* lacked an accessory pore (Faust, 1993b; Murray et al., 2007), but our SEM observations confirm its presence, although partially obscured by platelet protrusions (Fig.3e–g). In conclusion, *P. formosum* is unequivocally distinct from related species based on its unique platelet architecture (nine platelets with a wing-like structure on Platelet 1a), radial pore pattern, posterior nucleus, and molecular divergence. Morphologically similar *P. formosum* and *P. elegans* exhibited 0.134% (LSU rDNA) and 0.364% (ITS rDNA) genetic divergence, surpassing both the interspecific threshold (0.1%) and maximum intraspecific variability (0.3%) established for *Prorocentrum* (Zhang et al., 2007), confirming their distinct species status (Zhang et al., 2007). Phylogenetically, *P. formosum* forms a distinct clade, positioned as sister to taxa such as *P.* cf. *emarginatum*, *P. elegans*, and *P. rhathymum* (Fig.5). This distinct clustering supports its classification as an independent species.

4.2 The pigment of *P. formosum*

HPLC analysis of laboratory-cultured *P. formosum* (strain ZSG2) identified six pigments: chlorophyll *c* (chl *c*), peridinin, diadinoxanthin, chl *a*, peridinol, and diatoxanthin (Fig.7). Quantitative analysis revealed peridinin as the dominant carotenoid (0.133±0.010 mg/L), followed by chl *a* (0.098± 0.019 mg/L) and diadinoxanthin (0.095±0.008 mg/L). Many research results show that the major pigments in dinoflagellates are composed of peridinin, chl *a* and chl *c* (Hu et al., 1992; Zhang et al., 2007), but peridinin was the major carotenoid present in *Prorocentrum* cells (Faust et al., 1982; Hu et al., 1992; Krakhmalnyi et al., 2004; Hou et al., 2007; Berden-Zrimec et al., 2008). Different from the previous research results (Hu et al., 1992), the chl *c* detected in *P. formosum* was not the main pigment component compared with other pigments in the cell. The pigment component diatoxanthin was detected in *P. formosum*, *P. micans*, *P. cordatum*,

P. hoffmannianum, and *P. lima* in the genus of *Prorocentrum* (Faust et al., 1982; Krakhmalnyi et al., 2004; Hou et al., 2007; Berden-Zrimec et al., 2008), but not in *P. obtusidens* and *P. rhathymum* (Hu et al., 1992; Krakhmalnyi et al., 2004). The co-occurrence of diadinoxanthin and diatoxanthin indicates active operation of the photoprotective xanthophyll cycle, a mechanism triggered by high irradiance. This is corroborated by experimental evidence: diadinoxanthin-to-diatoxanthin conversion escalates under light stress in Alexandrium (Demers et al., 1991) and during late exponential growth phases in *Prorocentrum* (Faust et al., 1982; Hou et al., 2007; Berden-Zrimec et al., 2008). The presence of both diadinoxanthin and diatoxanthin in *P. formosum* may reflect its adaptation to benthic light environments influenced by tidal fluctuations. However, pigment composition alone cannot definitively resolve ecotype classification in *Prorocentrum*. Although the absence of diatoxanthin in some species and its presence in *P. formosum* imply divergent light acclimation strategies, this discrepancy may reflect microenvironmental light heterogeneity rather than obligate lifestyle differences (Faust et al., 1982; Krakhmalnyi et al., 2004; Hou et al., 2007; Berden-Zrimec et al., 2008).

5 CONCLUSION

In this study, we isolated *Prorocentrum formosum* from Anding Lianjiao (Contiguous Reef) (or Addington Shoal), Zhongsha Islands, confirmed its identity through morphology and molecular phylogeny. Genetic distances indicated closest affinity to *P. elegans*. Pigment analysis detected chlorophylls and xanthophylls but no okadaic acid. While non-toxic to *Artemia salina* and non-hemolytic, it caused moderate mortality in *Brachionus plicatilis*. This work provided the first molecular sequences for *P. formosum*.

6 DATA AVAILABILITY STATEMENT

The data that support the findings of this study are available from the corresponding author upon request.

7 ACKNOWLEDGMENT

We thank Dr. Heng CHEN from Wenzhou Medical University for his help in pigment composition analysis.

References

Alexander J, Benford D, Boobis A et al. 2019. Marine biotoxins in shellfish—Summary on regulated marine biotoxins. *The EFSA Journal*, **1306**: 1-23, https://doi.org/10.2903/j.efsa.2009.1306.

Aligizaki K, Nikolaidis G, Katikou P et al. 2009. Potentially toxic epiphytic *Prorocentrum* (Dinophyceae) species in Greek coastal waters. *Harmful Algae*, **8**(2): 299-311, https://doi.org/10.1016/J.HAL.2008.07.002.

Bauder A G, Cembella A D, Bricelj V M et al. 2001. Uptake and fate of diarrhetic shellfish poisoning toxins from the dinoflagellate *Prorocentrum lima* in the bay scallop *Argopecten irradians*. *Marine Ecology Progress Series*, **213**: 39-52, https://doi.org/10.3354/meps213039.

Berden-Zrimec M, Flander-Putrle V, Drinovec L et al. 2008. Growth, delayed fluorescence and pigment composition of four *Prorocentrum minimum* strains growing at two salinities. *Biological Research*, **41**(1): 11-23, https://doi.org/10.4067/S0716-97602008000100003.

Bialojan C, Rüegg J C, Takai A. 1988. Effects of okadaic acid on isometric tension and myosin phosphorylation of chemically skinned guinea-pig taenia coli. *The Journal of Physiology*, **398**(1): 81-95, https://doi.org/10.1113/jphysiol.1988.sp017030.

Chomérat N, Bilien G, Derrien A et al. 2019. *Ostreopsis lenticularis* Y. Fukuyo (Dinophyceae, Gonyaulacales) from French Polynesia (South Pacific Ocean): a revisit of its morphology, molecular phylogeny and toxicity. *Harmful Algae*, **84**: 95-111, https://doi.org/10.1016/j.hal.2019.02.004.

Chomérat N, Sellos D Y, Zentz F et al. 2010. Morphology and molecular phylogeny of *Prorocentrum consutum* sp. nov. (Dinophyceae), a new benthic dinoflagellate from South Brittany (northwestern France). *Journal of Phycology*, **46**(1): 183-194, https://doi.org/10.1111/j.1529-8817.2009.00774.x.

Chomérat N, Zentz F, Boulben S et al. 2011. *Prorocentrum glenanicum* sp. nov. and *Prorocentrum pseudopanamense* sp. nov. (Prorocentrales, Dinophyceae), two new benthic dinoflagellate species from South Brittany (northwestern France). *Phycologia*, **50**(2): 202-214, https://doi.org/10.2216/10-12.1.

David H, Laza-Martínez A, García-Etxebarria K et al. 2014. Characterization of *Prorocentrum elegans* and *Prorocentrum levis* (Dinophyceae) from the southeastern Bay of Biscay by morphology and molecular phylogeny. *Journal of Phycology*, **50**(4): 718-726, https://doi.org/10.1111/jpy.12200.

Demers S, Roy S, Gagnon R et al. 1991. Rapid light-induced changes in cell fluorescence and in xanthophyll-cycle pigments of *Alexandrium excavatum* (Dinophyceae) and *Thalassiosira pseudonana* (Bacillariophyceae): a photo-protection mechanism. *Marine Ecology Progress Series*, **76**(2): 185-193, https://doi.org/10.3354/meps076185.

Dodge J D. 1975. The Prorocentrales (Dinophyceae). II. Revision of the taxonomy within the genus *Prorocentrum*. *Botanical Journal of the Linnean Society*, **71**(2): 103-125, https://doi.org/10.1111/j.1095-8339.1975.tb02449.x.

Edgar R C. 2004. MUSCLE: multiple sequence alignment with high accuracy and high throughput. *Nucleic Acids Research*, **32**(5): 1792-1797, https://doi.org/10.1093/nar/gkh340.

Faust M A, Sager J C, Meeson B W. 1982. Response of *Prorocentrum mariae-lebouriae* (Dinophyceae) to light of different spectral qualities and irradiances: growth and pigmentation. *Journal of Phycology*, **18**(3): 349-356, https://doi.org/10.1111/j.1529-8817.1982.tb03195.x.

Faust M A. 1990. Morphologic details of six benthic species of *Prorocentrum* (Pyrrophyta) from a mangrove island, Twin Cays, Belize, including two new species. *Journal of Phycology*, **26**(3): 548-558, https://doi.org/10.1111/j.0022-3646.1990.00548.x.

Faust M A. 1991. Morphology of ciguatera-causing *Prorocentrum lima* (Pyrrophyta) from widely differing sites. *Journal of Phycology*, **27**(5): 642-648, https://doi.org/10.1111/j.0022-3646.1991.00642.x.

Faust M A. 1993a. Three new benthic species of *Prorocentrum* (Dinophyceae) from Twin Cays, Belize: *P. maculosum* sp. nov., *P. foraminosum* sp. nov. and *P. formosum* sp. nov. *Phycologia*, **32**(6): 410-418, https://doi.org/10.2216/i0031-8884-32-6-410.1.

Faust M A. 1993b. *Prorocentrum belizeanum*, *Prorocentrum elegans*, and *Prorocentrum caribbaeum*, three new benthic species (Dinophyceae) from a mangrove island, Twin Cays, Belize. *Journal of Phycology*, **29**(1): 100-107, https://doi.org/10.1111/j.1529-8817.1993.tb00287.x.

Faust M A, Vandersea M W, Kibler S R et al. 2008. *Prorocentrum levis*, a new benthic species (Dinophyceae) from a mangrove island, Twin Cays, Belize. *Journal of Phycology*, **44**(1): 232-240, https://doi.org/10.1111/j.1529-8817.2007.00450.x.

Fukuyo Y. 1981. Taxonomical study on benthic dinoflagellates collected in coral reefs. *Bulletin of the Japanese Society of Scientific Fisheries*, **47**(8): 967-978, https://doi.org/10.2331/suisan.47.967.

Gómez F, Gast R J. 2022. Rediscovery of the gonyaulacoid dinoflagellate *Schuettiella*. *The Journal of Eukaryotic Microbiology*, **69**(4): e12920, https://doi.org/10.1111/jeu.12920.

Grzebyk D, Sako Y, Berland B. 1998. Phylogenetic analysis of nine species of *Prorocentrum* (Dinophyceae) inferred from 18S ribosomal DNA sequences, morphological comparisons, and description of *Prorocentrum panamensis*, sp. nov. *Journal of Phycology*, **34**(6): 1055-1068, https://doi.org/10.1046/j.1529-8817.1998.341055.x.

Guiry M D, Guiry G M. 2025. AlgaeBase. World-wide electronic publication, National University of Ireland, Galway, https://www.algaebase.org.

Han M S, Wang P B, Kim J H et al. 2016. Morphological and molecular phylogenetic position of *Prorocentrum micans* sensu stricto and description of *Prorocentrum koreanum* sp. nov. from southern coastal waters in Korea and Japan. *Protist*, **167**(1): 32-50, https://doi.org/10.1016/j.protis.2015.12.001.

Hoppenrath M, Chomerat N, Horiguchi T et al. 2013. Taxonomy and phylogeny of the benthic *Prorocentrum* species (Dinophyceae)—A proposal and review. *Harmful Algae*, **27**: 1-28, https://doi.org/10.1016/j.hal.2013.03.006.

Hou J J, Huang B Q, Cao Z R et al. 2007. Effects of nutrient limitation on pigments in *Thalassiosira weissflogii* and *Prorocentrum donghaiense*. *Journal of Integrative Plant Biology*, **49**(5): 686-697, https://doi.org/10.1111/j.1744-7909.2007.00449.x.

Hu T M, Marr J, de Freitas A S W et al. 1992. New diol esters isolated from cultures of the dinoflagellates *Prorocentrum lima* and *Prorocentrum concavum*. *Journal of Natural Products*, **55**(11): 1631-1637, https://doi.org/10.1021/np50089a011.

Krakhmalnyi A F, Tishaeva M V, Panina Z A et al. 2004. A problem on identity *Prorocentrum cordatum* (Ostf.) Dodge and *P. minimum* (Pavill.) Schiller (*Dinophyta*). *International Journal on Algae*, **6**(4): 331-340, https://doi.org/10.1615/InterJAlgae.v6.i4.30.

Kumar S, Stecher G, Li M et al. 2018. MEGA X: molecular evolutionary genetics analysis across computing platforms. *Molecular Biology and Evolution*, **35**(6): 1547-1549, https://doi.org/10.1093/molbev/msy096.

Leander B S, Hoppenrath M. 2008. Ultrastructure of a novel tube-forming, intracellular parasite of dinoflagellates: *Parvilucifera prorocentri* sp. nov. (Alveolata, Myzozoa). *European Journal of Protistology*, **44**(1): 55-70, https://doi.org/10.1016/j.ejop.2007.08.004.

Lim Z F, Luo Z H, Lee L K et al. 2019. Taxonomy and toxicity of *Prorocentrum* from Perhentian Islands (Malaysia), with a description of a non-toxigenic species *Prorocentrum malayense* sp. nov. (Dinophyceae). *Harmful Algae*, **83**: 95-108, https://doi.org/10.1016/j.hal.2019.01.007.

Loeblich A R III, Sherley J L, Schmidt R J. 1979. The correct position of flagellar insertion in *Prorocentrum* and description of *Prorocentrum rhathymum* sp. nov. (Pyrrhophyta). *Journal of Plankton Research*, **1**(2): 113-120, https://doi.org/10.1093/plankt/1.2.113.

Louzao M C, Fernández D A, Abal P et al. 2015. Diarrhetic effect of okadaic acid could be related with its neuronal action: changes in neuropeptide Y. *Toxicology Letters*, **237**(2): 151-160, https://doi.org/10.1016/j.toxlet.2015.06.004.

Lundholm N, Bernard C, Churro C et al. 2025. IOC-UNESCO Taxonomic Reference List of Harmful Micro Algae. https://www.marinespecies.org/hab, https://doi.org/10.14284/362.

Luo Z H, Zhang H, Krock B et al. 2017. Morphology, molecular phylogeny and okadaic acid production of epibenthic *Prorocentrum* (Dinophyceae) species from the northern South China Sea. *Algal Research*, **22**: 14-30, https://doi.org/10.1016/j.algal.2016.11.020.

Mohammad-Noor N, Moestrup Ø, Daugbjerg N. 2007. Light, electron microscopy and DNA sequences of the dinoflagellate *Prorocentrum concavum* (syn. *P. arabianum*) with special emphasis on the periflagellar area. *Phycologia*, **46**(5): 549-564, https://doi.org/10.2216/06-94.1.

Murray S, Nagahama Y, Fukuyo Y. 2007. Phylogenetic study of benthic, spine-bearing prorocentroids, including *Prorocentrum fukuyoi* sp. nov.. *Phycological Research*, **55**(2): 91-102, https://doi.org/10.1111/j.1440-1835.2007.00452.x.

Nascimento S M, Mendes M C Q, Menezes M et al. 2017. Morphology and phylogeny of *Prorocentrum caipirignum*

sp. nov. (Dinophyceae), a new tropical toxic benthic dinoflagellate. *Harmful Algae*, **70**: 73-89, https://doi.org/10.1016/j.hal.2017.11.001.

Nishimura T, Uchida H, Noguchi R et al. 2020. Abundance of the benthic dinoflagellate *Prorocentrum* and the diversity, distribution, and diarrhetic shellfish toxin production of *Prorocentrum lima* complex and *P. caipirignum* in Japan. *Harmful Algae*, **96**: 101687, https://doi.org/10.1016/j.hal.2019.101687.

Page R D M. 1996. Tree View: an application to display phylogenetic trees on personal computers. *Bioinformatics*, **12**(4): 357-358, https://doi.org/10.1093/bioinformatics/12.4.357.

Pin L C, Teen L P, Ahmad A et al. 2001. Genetic diversity of *Ostreopsis ovata* (Dinophyceae) from Malaysia. *Marine Biotechnology*, **3**(3): 246-255, https://doi.org/10.1007/s101260000073.

Ronquist F, Huelsenbeck J P. 2003. Mrbayes 3: Bayesian phylogenetic inference under mixed models. *Bioinformatics*, **19**(12): 1572-1574, https://doi.org/10.1093/bioinformatics/btg180.

Scholin C A, Herzog M, Sogin M et al. 1994. Identification of group- and strain-specific genetic markers for globally distributed *Alexandrium* (Dinophyceae). II. Sequence analysis of a fragment of the LSU rRNA gene. *Journal of Phycology*, **30**(6): 999-1011, https://doi.org/10.1111/j.0022-3646.1994.00999.x.

Stamatakis A. 2014. RAxML version 8: a tool for phylogenetic analysis and post-analysis of large phylogenies. *Bioinformatics*, **30**(9): 1312-1313, https://doi.org/10.1093/bioinformatics/btu033.

Takai A, Murata M, Torigoe K et al. 1992. Inhibitory effect of okadaic acid derivatives on protein phosphatases. A study on structure-affinity relationship. *The Biochemical Journal*, **284**(Pt 2): 539-544, https://doi.org/10.1042/bj2840539.

Tillmann U, Hoppenrath M, Gottschling M. 2019. Reliable determination of *Prorocentrum micans* Ehrenb. (Prorocentrales, Dinophyceae) based on newly collected material from the type locality. *European Journal of Phycology*, **54**(3): 417-431, https://doi.org/10.1080/09670262.2019.1579925.

Tomas C R. 1996. Identifying Marine Diatoms and Dinoflagellates. Academic Press, San Diego.

Vale C, Botana L M. 2008. Marine toxins and the cytoskeleton: okadaic acid and dinophysistoxins. *The FEBS Journal*, **275**(24): 6060-6066, https://doi.org/10.1111/j.1742-4658.2008.06711.x.

Verma A, Kazandjian A, Sarowar C et al. 2019. Morphology and phylogenetics of benthic *Prorocentrum* species (Dinophyceae) from tropical northwestern Australia. *Toxins*, **11**(10): 571, https://doi.org/10.3390/toxins11100571.

Wang X, Liu C, Zhang Q C et al. 2023. A dinoflagellate bloom caused by multiple species of Kareniaceae in the coastal waters of Fujian in June 2022 and its adverse impacts on *Brachionus plicatilis* and *Artemia salina*. *Marine Pollution Bulletin*, **196**: 115685, https://doi.org/10.1016/j.marpolbul.2023.115685.

Zapata M, Rodríguez F, Garrido J L. 2000. Separation of chlorophylls and carotenoids from marine phytoplankton: a new HPLC method using a reversed phase C8 column and pyridine-containing mobile phases. *Marine Ecology Progress Series*, **195**: 29-45, https://doi.org/10.3354/meps195029.

Zhang H, Bhattacharya D, Lin S J. 2007. A three-gene dinoflagellate phylogeny suggests monophyly of Prorocentrales and a basal position for *Amphidinium* and *Heterocapsa*. *Journal of Molecular Evolution*, **65**(4): 463-474, https://doi.org/10.1007/s00239-007-9038-4.

Zhang H, Li Y, Cen J Y et al. 2015. Morphotypes of *Prorocentrum lima* (Dinophyceae) from Hainan Island, South China Sea: morphological and molecular characterization. *Phycologia*, **54**(5): 503-516, https://doi.org/10.2216/15-8.1.

Zhou C X, Fu Y J, Yan X J. 2007. Hemolytic activity studies of several harmful alga strains. *Asian Journal of Ecotoxicology*, **2**(1): 78-82, https://doi.org/10.3969/j.issn.1673-5897.2007.01.011. (in Chinese with English abstract)

Zou J, Li Q, Liu H et al. 2022. Taxonomy and toxin profile of harmful benthic *Prorocentrum* (Dinophyceae) species from the Xisha Islands, South China Sea. *Journal of Oceanology and Limnology*, **40**(3): 1171-1190, https://doi.org/10.1007/s00343-021-1045-6.

Zou J, Li Q, Lu S H et al. 2020. The first benthic harmful dinoflagellate bloom in China: morphology and toxicology of *Prorocentrum concavum*. *Marine Pollution Bulletin*, **158**: 111313, https://doi.org/10.1016/j.marpolbul.2020.111313.